energies

MDPI

Article

Correlation Characteristics Comparison of SF_6 Decomposition versus Gas Pressure under Negative DC Partial Discharge Initiated by Two Typical Defects

Dong Yang [1], Ju Tang [1], Xu Yang [1], Ke Li [1], Fuping Zeng [1,*], Qiang Yao [2], Yulong Miao [2] and Lincong Chen [3]

1 School of Electrical Engineering, Wuhan University, Wuhan 430072, China; scyangdong@163.com (D.Y.); whtangju@whu.edu.cn (J.T.); 15102738342@126.com (X.Y.); whulike@126.com (K.L.)
2 Electric Power Research Institute, Chongqing Power Company, Chongqing 401123, China; 2012202070085@whu.edu.cn (Q.Y.); ygxflyhigh@163.com (Y.M.)
3 Electric Power Research Institute, Hainan Power Grid Co., Ltd., Haikou 570100, China; xuanxie163@163.com
* Correspondence: Fuping.Zeng@whu.edu.cn; Tel.: +86-027-6877-2323

Received: 19 June 2017; Accepted: 21 July 2017; Published: 25 July 2017

Abstract: Aimed to clarify the correlation characteristics between the internal partial discharge (PD) in negative direct current (DC) gas insulated system (GIS) and gas pressure initiated by two typical defects (i.e., free-metal particles and metal protrusion), this study on PD decomposition of sulfur hexafluoride (SF_6) was investigated under different pressures on the basis of constructing a SF_6 decomposition experimental platform with DC PD. Free-metal particles and metal protrusion in a GIS were simulated using a spherical-bowl electrode and a needle-plate electrode, respectively. Trends and differences in the performance of SF_6 decomposition components SOF_2, SO_2F_2, CO_2, and SO_2 at different pressures were compared and analyzed by experiments under different defects. Based on gas microscopic ionization theory, the relationship between the decomposition component and gas pressure was deduced and verified. The concentrations of different decomposition components were found to vary with the change in gas pressure under different defects, whereas the characteristic ratios of decomposition components versus gas pressure showed a similar trend.

Keywords: SF_6; partial discharge (PD); direct current (DC); gas pressure; metal protrusion defect; free metal particles defect

1. Introduction

With the large-scale renewable energy access and the application of flexible direct current (DC) transmission technology [1], DC gas insulated system (GIS) equipment has been widely investigated aiming at improving the reliability of the power system and reducing the space occupied by the equipment [2,3]. However, GIS inevitably encounter different levels of insulation defects in design, manufacturing, transportation, installation, operation, and maintenance. In time, these insulation defects may escalate into insulation failure during operation, thus posing a risk to the safe and reliable operation of the equipment and the entire power grid [4]. Extensive studies [5,6] have reported that the SF_6 molecules crack to form low fluoride (SF_x, x = 1, ..., 5) under partial discharge (PD) [5,6]. After long-term operation, different levels of trace moisture, oxygen, and other impurities may be present inside of GIS. SF_x will react with impurities to form new components, which can result in the deterioration of the insulation. The generated components are closely related to the internal fault factors. The decomposed components analysis (DCA) method, which is based on the generation of and variation in these characteristic components, can be used in condition monitoring and fault diagnosis of SF_6 gas insulation equipment [7].

The physical and chemical processes of SF_6 decomposition under PD are very complex, because many factors influence the decomposition, such as discharge energy, electrode material, trace oxygen, trace water, and gas pressure. Most of the previous studies have focused on the influence of discharge energy, electrode material, trace oxygen, and trace water [8–10]. Only a few studies have conducted a qualitative research and description on the effect of pressure [11,12]. Moreover, the aforementioned research primarily focused on the characteristics of alternating current (AC) GIS under PD decomposition initiated by metal protrusion, and does not extend to the DC field and other typical defects. According to statistics, free metal particles and metal protrusion defects are encountered at the forefront of insulation defects from the point of triggering GIS failure rates [4]. Gas pressure in GIS varies with the room temperature, and the gas pressure of SF_6 gas insulation equipment at different voltage levels varies as well. Therefore, investigating the relationship between gas pressure and the SF_6 decomposition component under free metal particles and metal protrusion defects can elucidate the SF_6 gas decomposition mechanism, and provide a theoretical basis for gas pressure effect modification when diagnosing the insulation fault by DCA.

In the present work, defects caused by free-metal particles and metal protrusion were simulated by spherical-bowl electrode and needle-plate electrode, respectively, based on the SF_6 DC PD decomposition experiment platform. Formation data of SOF_2, SO_2F_2, CO_2, and SO_2 were obtained by experiments under 0.2 MPa, 0.25 MPa, 0.3 MPa, 0.35 MPa, and 0.4 MPa, respectively. This paper systematically studied the variation mechanism of SF_6 decomposition component versus gas pressure under different defects by experimentation and theory. Our results provided a theoretical and experimental basis for using SF_6 decomposition products to identify gas insulation equipment failure and to assess its state of insulation.

2. SF_6 DC PD Decomposition Experiment

2.1. Experimental Research Platform

The SF_6 DC PD decomposition experimental device is shown in Figure 1. The regulator (T_1: 0–380 V) and the experimental transformer (T_2: 50 kVA/100 kV) provided the AC high voltage to the circuit. The half-wave rectifier circuit composed by the high voltage silicon stack (D: 100 kV/5 A) and the filter capacitor (C_1: 0.2 μF) converted AC voltage into a negative DC voltage, which was applied on the insulation defect. Protection resistors (R_1: 10 kΩ) and (R_2: 20 kΩ) limited the current at breakdown to protect the entire experimental device. C_v and R_v were used as a capacitive voltage divider and resistance divider to measure the AC and DC voltage, respectively. The above devices were made by Hdbl Company, Wuhan, China. Coupling capacitance (C_k: 500 pF/100 kV), non-inductance resistor (Z_m: 50 Ω), and digital storage oscilloscope (DSO) were used to measure discharge magnitude. The characteristic components of SF_6 were separated and quantitatively detected using Shimadzu QP-2010Ultra gas chromatography (GC/MS) with special capillary column (CP-Sil5CB). The specific experimental steps are described in references [10,12].

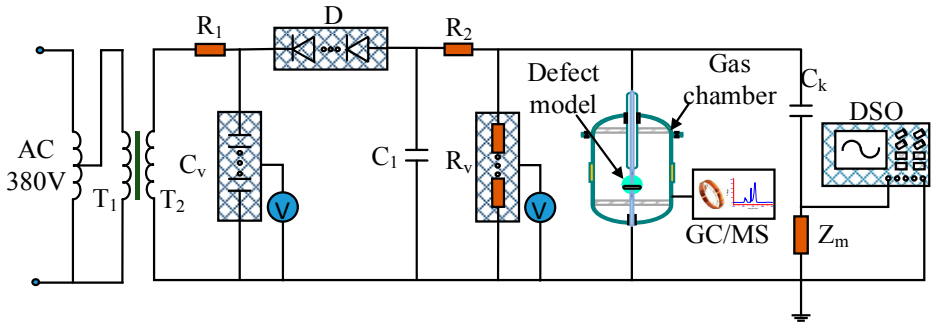

Figure 1. SF_6 decomposition test wiring diagram under DC PD.

2.2. Experimental Content

2.2.1. Defect Model

The experiment had to overcome the problem of experimental data dispersion caused by the decrease of particles during test, as well as to simulate an axisymmetric and mostly uniform field between the real GIS equipment shell and the high voltage (HV) conductor. Free-metal particles defect in GIS devices was were simulated by 20 six-series aluminum alloy balls with a diameter of 3 mm [13], which are located in a spherical bowl electrode, as shown in Figure 2a. The bowl was cut with a hollow stainless steel sphere (Φ = 100 mm). The cut diameter was 90 mm, which enabled the jumping aluminum balls to fall back into the bowl electrode effectively and thus prevented the decrease in number of aluminum balls during the experiment and stabilize the experimental data.

The metal protrusion defect was simulated by a stainless steel needle–plate electrode. The distance between the needle and plate was 10 mm. The diameter of the plate electrode was 100 mm, and the curvature radius of the needle electrode tip was 0.3 mm. The physical model of the metal protrusion defect is shown in Figure 2b.

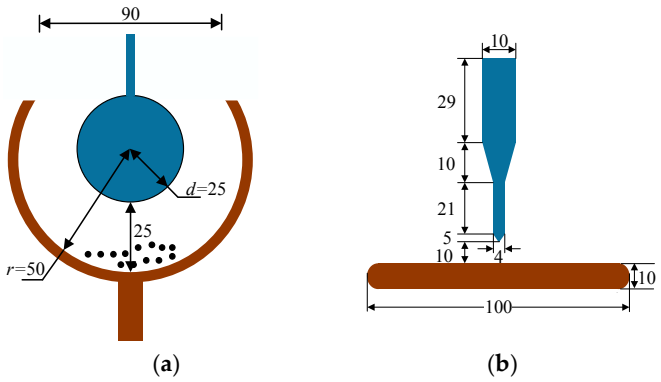

Figure 2. Dimensional structure of defect model: (**a**) Free metal particles defect and (**b**) metal protrusion defect (Unit: mm).

2.2.2. Experiment Conditions

The operation pressure of SF_6 DC GIS (such as in medium- and low-pressure wall bushing, and switchgear cabinet) is generally less than 0.4 MPa. The pressure of laboratory equipment is 0.1–0.4 MPa. Considering the above information and the current experimental conditions, five SF_6 absolute pressure were applied, namely, 0.2, 0.25, 0.3, 0.35, and 0.4 MPa. To ensure experimental accuracy, all experiments were conducted in room temperature of 20 °C, and a relative humidity of 40%. The concentrations of trace water and trace oxygen in every experiment were maintained at about 40 μmol/L and 70 μmol/L to ensure that the experimental conditions are consistent. During the experiment, the applied voltage were 60 kV to the needle-plate electrode, and 48 kV to spherical-bowl. PD decomposition experiments were carried out for 96 h in each group. Samples were collected at 12 h intervals and quantitatively analyzed by GC/MS. The SF_6 was quantitatively analyzed at 0 h before every experiment to obtain the concentration impurities that may remain in the chamber during the previous experiment. The concentrations of SF_6 decomposition components in this paper are net production which has been subtracted from the 0 h background of impurities. To verify the reproducibility of the experiment, all experiments were carried out twice under the same experimental conditions in this paper. The experimental data were averaged for two of the experimental data.

And the maximum relative mean deviation RSD_{max} of each group of data at same discharge time is used to illustrate the reproducibility of the experimental data.

$$RSD_{max} = \max\left[\frac{|x_i^1 - \overline{x}_i| + |x_i^2 - \overline{x}_i|}{\overline{x_i}}\right] i = 0.2\,\text{Mpa},\ 0.25\,\text{Mpa},\ \ldots.0.4\,\text{Mpa} \quad (1)$$

where, x_i^1 is the first measured data under the i pressure; x_i^2 is the second measured data under the i pressure; $\overline{x}_i$ is averaged for two measured data under the i pressure. RSD_{max} is the maximum value of the five groups of pressure at the same discharge time.

3. Change Trend in SF_6 Decomposition Components versus Gas Pressure

Considering constant volume, an increasing pressure of the reaction chamber was increased to change the molar concentration of the gas in the chamber, which in turn affected the progress of the chemical reaction. However, GC/MS detects the volume fraction of the gas (μL/L), which cannot directly reflect the change in the absolute generation of decomposition components in the gas chamber. Therefore, the volume fraction of gas was converted into molar concentration prior to analysis. Given that the experimental chamber was about 60 L, only a small amount of gas was collected to quantitatively detect decomposition products every 12 h. In addition, the SF_6 decomposition ratio was very small, and thus, the change in gas pressure can be neglected. The conversion formula between volume fraction of decomposition components and the concentration is shown in Equation (2).

$$c_i = \frac{p_i}{RT} v_i \quad (2)$$

where, c_i is the concentration of component (μmol/L); p_i is the gas pressure of the experiment chamber; R is the gas constant; T is the room temperature; and v_i is the volume fraction of component.

The types and amount of decomposition components under the two typical defects at 96 h were shown in Figure 3. SF_6 were decomposed into CO_2, SO_2F_2, SOF_2, and SO_2 in five groups of different gas pressure experiment under both metal protrusion defect and free-metal particles defect. The yield relationship of metal protrusion defect is $SOF_2 > SO_2F_2 > CO_2 > SO_2$ under different gas pressures. The concentrations of SO_2F_2 and SOF_2 were much higher than the others, which is the main decomposition product under the metal protrusion defect. The yield relationship of free-metal particles defect under different pressures presented a different relationship. When 0.2 MPa $\leq p \leq$ 0.25 MPa, $SOF_2 > SO_2F_2 > CO_2 > SO_2$; when 0.3 MPa $\leq p \leq$ 0.35 MPa, $SOF_2 > CO_2 > SO_2F_2 > SO_2$; when p = 0.4 MPa, $SOF_2 > CO_2 > SO_2 > SO_2F$. The concentrations of SOF_2 are much higher than others. The average single discharge energy of metal protrusion defect at different pressures were 1.53×10^{-5} J, 1.49×10^{-5} J, 1.49×10^{-5} J, 1.38×10^{-5} J, 1.34×10^{-5} J, respectively. The average single discharge energy of free metal particles defect were 9.99×10^{-5} J, 1×10^{-4} J, 8.67×10^{-5} J, 8.2×10^{-5} J, 7.54×10^{-5} J.

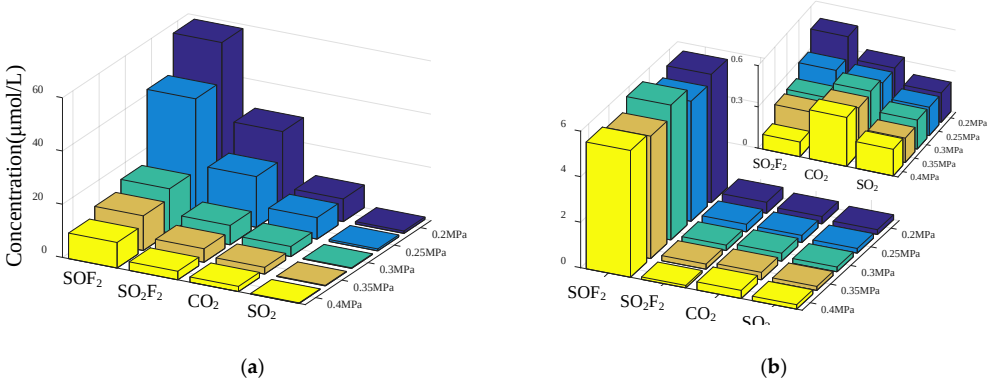

Figure 3. Concentration of SF_6 decomposed components at 96 h: (**a**) Protrusion and (**b**) particles.

3.1. Change Trend in SF_6 Decomposition Component Content versus Gas Pressure

3.1.1. The Characteristics of the Changes in SOF_2 Concentration versus Gas Pressure

The relationship of SOF_2 concentration versus pressure is shown in Figure 4. The generation concentration of SOF_2 exhibits an inverse "S" curve with increasing gas pressure within the same PD time initiated by the metal protrusion defect. The change curve of SOF_2 concentration versus gas pressure can be divided into three periods: Saturated area, Exponent area, and Flat area. When the gas pressure is at 0.2 MPa $\leq p \leq$ 0.25 MPa, the energy obtained by the particle in the electric field decreases as gas pressure increases. Furthermore, the probability of the excitation or ionization of the gas molecules caused by collision decreased; the formation of SOF_2 gradually declines. When gas pressure is at 0.2 MPa, the longer mean free path can lead to further particle collision reaction. However, the concentrations of H_2O and O_2 in the chamber inhibited SOF_2 formation. With the increase in gas pressure, the collision ionization is gradually reduced. The inhibition of trace amounts of H_2O and O_2 was also gradually weakened. Consequently, the slope between the generation concentration of SOF_2 and gas pressure gradually increased. With decreased gas pressure to nearly 0.25 MPa, the inhibitory effect of trace amounts of H_2O and O_2 on SOF_2 formation became negligible. Hence, the 0.2 MPa $\leq p \leq$0.25 MPa stage can be called the Saturated Area. In addition, when the pressure further increases to 0.3 MPa, the generation of SOF_2 is primarily related to the amount of SF_6 ionization decomposition. At this stage, the reduction of the electron mean free path leads to a significant reduction of the particle energy and drastically reduces and the possibility of SF_6 collision ionization is sharply reduced. Therefore, the SOF_2 generation concentration is rapidly reduced with increased gas pressure. This stage can be called the Exponent Area. When the gas pressure is in within the range of 0.3 MPa $\leq p \leq$ 0.4 MPa, the mean free path was very small compared with the Exponent Area. At this stage, the probability that the electron free path was greater than the required path of the collision ionization slowly reduced [14]. The formation concentration of SOF_2 was also gradually reduced, and its slope with the gas pressure is less than the Exponent Area. This stage can be called the Flat Area.

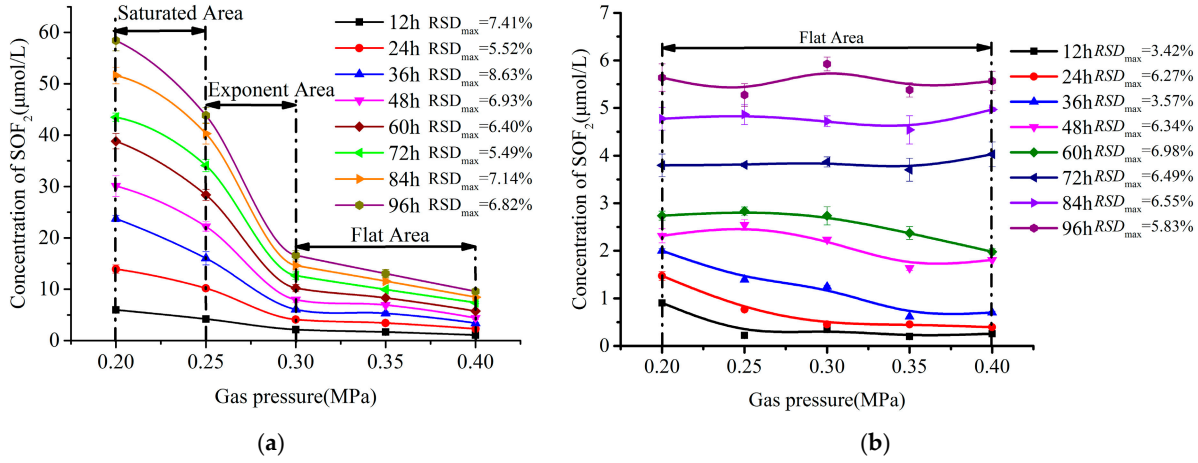

Figure 4. Correlation between SOF_2 concentration and pressure: (**a**) Protrusion and (**b**) particles.

With the free-metal particles defect, SOF_2 generation concentration almost did not change with the increase in gas pressure, and remained in the Flat Area. SOF_2 is usually derived from the hydrolysis of SF_4. SO_2F_2 mainly comes from the reaction of SF_2 and O_2 [15]. The energy required for SF_4 generation is lower than that required for SF_2, which indicates that the effect of increased pressure on lower energy discharge is weak in the free-metal particles defect. This result can be explained as follows: the metal protrusion defect can maintain a stable electric field distortion for a long time. The electrons need to be accelerated by a long distance to get enough energy and achieve SF_6 collision ionization. The gas

pressure affects the electron mean free path, therefore affecting its PD process. Hence, the formation of components under the defect is significantly affected by the pressure. In the free-metal particles defect, free particles that have induced enough charge to overcome its own gravity take off and collide with the ball electrode. The process of generating the induced charge is weakly affected by the gas pressure. In addition, the electric field exhibits serious distortion and PD occurs when the particles are very close to the electrode. The discharge time is very short and the discharge is violent. The average single discharge energy in the free metal particles defect at 0.4 Mpa was much greater than the metal protrusion, which indicates that the electrons can obtain a certain amount of energy even at higher pressure under free metal particles defect. Therefore, under this defect, the change in gas pressure has less effect on the lower energy discharge.

3.1.2. The Change Characteristic of SO_2 Concentration versus Gas Pressure

The relationship of SOF_2 concentration versus gas pressure under the two typical defects is presented in Figure 5. SO_2 is mainly derived from the hydrolysis of SOF_2 [15]. The relationship of its concentration versus gas pressure is similar to that of SOF_2. This relationship can be divided into three periods as well, namely, Saturated Area, Exponent Area, and Flat Area under the metal protrusion defect. In the free-metal particles, the concentrations observed all fall under the Flat Area.

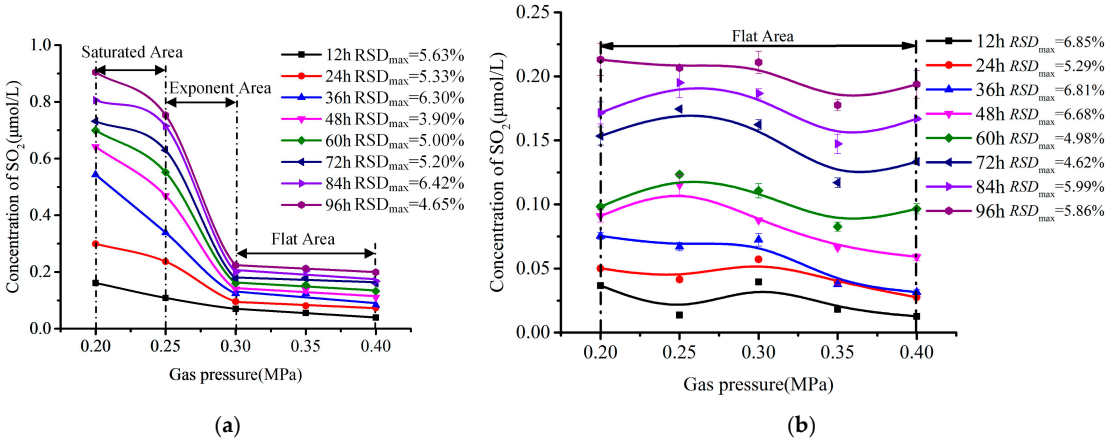

Figure 5. Correlation between SO_2 concentration and pressure: (**a**) Protrusion and (**b**) particles.

3.1.3. The Change Characteristic of CO_2 Concentration versus Gas Pressure

The relationship between CO_2 concentration and gas pressure in the two typical defects is presented in Figure 6. The generation concentration of CO_2 exhibits an inverse "S" curve with increased gas pressure within the same PD time initiated by metal protrusion defect. The change curve of SOF_2 concentration versus gas pressure can be divided into three periods: Saturated Area, Exponent Area, and Flat Area. When the gas pressure is within the range of 0.2 MPa $\leq p \leq$ 0.25 MPa, CO_2 formation is inhibited by the concentrations of H_2O and O_2 and thus the formation of CO_2 does not increase rapidly with the decrease in gas pressure. When the gas pressure increases and approaches 0.25 MPa, the limits of H_2O and O_2 are no longer significant. At this stage, the collision ionization and the concentration of CO_2 decreases rapidly with the increase in gas pressure. As the gas pressure further increases, the inflection point of the curve appears near 0.3 MPa. Similar to the change curve of concentration of SOF_2 in the Flat Area, the number of excited C particles slowly declines as gas pressure increases, compared with Exponent area and the increase in gas pressure. This stage is called the Flat Area.

In the free-metal particle defects, the concentration of CO_2 is almost constant with increased gas pressure, falling in the Flat Area. This phenomenon can be compared to the reason for the formation of SOF_2 in free-metal particles, which suggests that the energy required for CO_2 formation is also low.

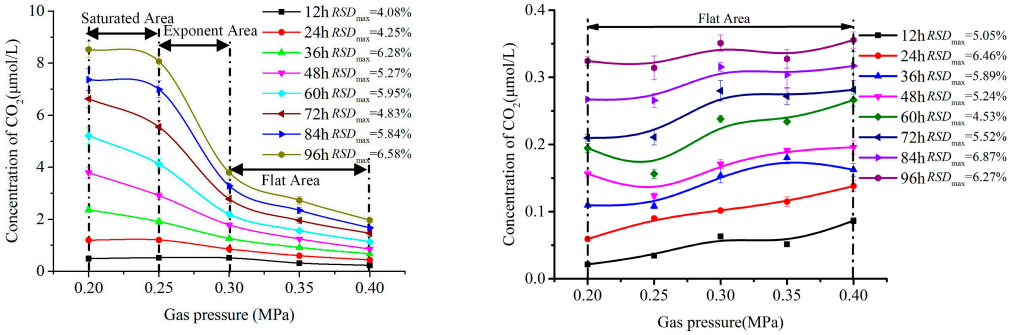

Figure 6. Correlation between CO_2 concentration and pressure: (**a**) Protrusion and (**b**) particles.

3.1.4. The Change Characteristic of SO_2F_2 Concentration versus Gas Pressure

The relationship between SOF_2 concentration and gas pressure in the two typical defects is presented in Figure 7. The concentration of SO_2F_2 is less than that of SOF_2 for the energy of SO_2F_2 formation is larger than of SOF_2 [15].

In the same PD time caused by the metal protrusion, the concentration of SO_2F_2 versus increased gas pressure shows an inverted "*J*" type curve relationship, which is different from the concentration of SOF_2 with increased gas pressure, which exhibits an inverse "S" curve relationship. That is, the change curve of SOF_2 generation concentration versus the pressure can be divided into two periods: Exponent Area and Flat Area. As shown in Figures 4a and 7a, both the Flat and Exponent Areas appear in the correlation curves of SOF_2 and SO_2F_2 versus the pressure whose cause is similar, but the curve of the SO_2F_2 concentration versus the gas pressure does not appear in the Saturated Area. This result is explained as follows: the concentration of H_2O and O_2 in the gas chamber limits the formation of SOF_2 and CO_2 and enters the Saturated Area at 0.2 MPa $\leq p \leq$ 0.25 MPa. However, SF_2 has a much stronger reducibility than SF_4 and C. Consequently, O atoms are easily obtained for SF_2, which makes SO_2F_2 formation at this stage remaining in the Exponent Area.

Under the free-metal particles defect, the concentration of SO_2F_2 decreases rapidly with increased gas pressure, which all falls under the Exponent Area. From the previous analysis of the free-metal particles defect, electrons obtain some energy even under high gas pressure. The change in gas pressure has little effect on the low-energy discharge in the PD caused by the defect. However, the formation of SF_2 requires SF_6 to break four S-F bonds at the same time, which requires considerable energy. Electrons need to go through enough free paths to obtain enough energy and cause the decomposition of SF_6. Thus, the formation of SO_2F_2 was considerably affected by gas pressure. Its concentration deceases rapidly along with an increase in gas pressure. The change in gas pressure significantly affected on the higher energy discharge under metal free particle defects.

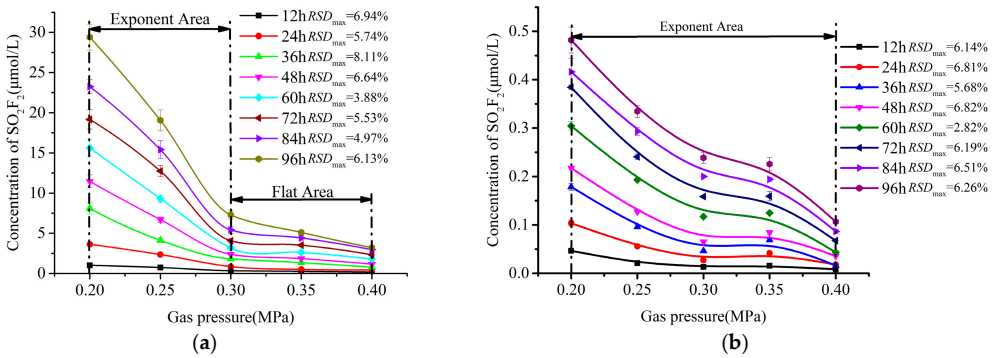

Figure 7. Correlation between SO_2F_2 concentration and pressure: (**a**) Protrusion and (**b**) particles.

3.2. Change Characteristics of the Characteristic Components Ratios versus Gas Pressure

The ratio method has been widely used in the power equipment fault diagnosis as this method can prevent the influence of volume effect on the fault diagnosis results. In this paper, the effect of gas pressure on the ratio of two decomposition components, namely, c (SO_2F_2)/c (SOF_2 + SO_2) and c (CF_4 + CO_2)/c (SO_2F_2 + SOF_2 + SO_2), is studied under negative DC. The effective characteristic ratio (CR_{RMS}) is used to study SF_6 decomposition characteristics under different gas pressures to achieve significant statistical results [8]. CR_{RMS} is defined as follows:

$$CR_{RMS} = \sqrt{\frac{1}{n}\sum_{m=1}^{n}\left(\frac{C_{im}}{C_{jm}}\right)^2} \tag{3}$$

where C_{im} and C_{jm} are the concentrations of components i and j, respectively, measured at mth time. n is the number of times after the characteristic ratio reaches the steady state.

As shown in Figure 8, the effective characteristic ratios of c (SO_2F_2)/c (SOF_2 + SO_2) under two typical defects decrease mostly linearly along with increased gas pressure. Given that the formation of SO_2F_2 consumes more energy than SOF_2, this reaction inhibits the formation of SO_2F_2, with increased gas pressure, which reduces the energy acquired by electrons. Therefore, c (SO_2F_2)/c (SOF_2 + SO_2) continues to decrease. Moreover, the effective concentration ratio c (CO_2)/c (SO_2F_2 + SOF_2 + SO_2) gradually increases along with gas pressure, and remains stable after reaching 0.3 MPa. Therefore, this conclusion shows that there is no significant change of c (CO_2)/c (SO_2F_2 + SOF_2 + SO_2) in the GIS whose gas pressure ranges from 0.3 to 0.4 MPa.

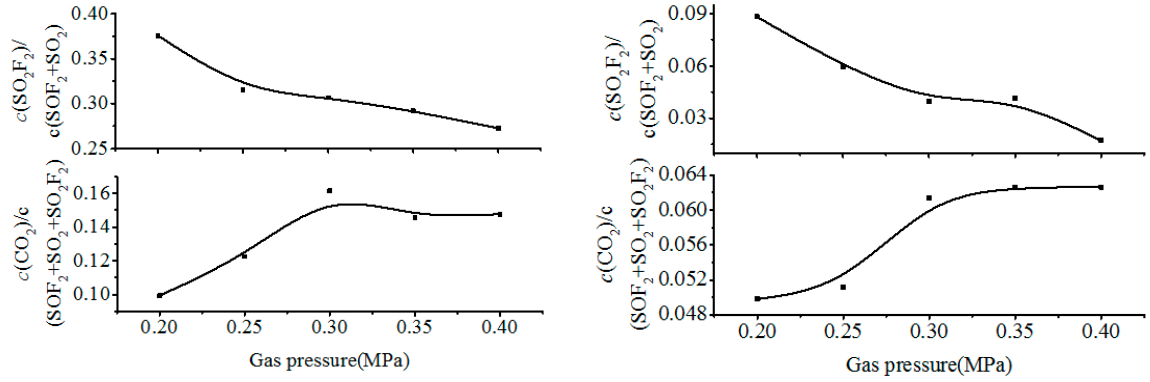

(**a**) (**b**)

Figure 8. Correlation curve of effective concentration ratios of characteristic component versus gas pressure: (**a**) Protrusion and (**b**) particles.

4. Quantitative Analysis of Gas Pressure on SF_6 Decomposition

Chen C.L. [16] reported that given the relatively low PD energy caused by insulation defects in an SF_6 gas insulation equipment, the difference in temperature change in the relevant area is not obvious. Therefore, the main reason for the decomposition of SF_6 gas is the strong distortion electrical field. Considering the role of electrons as a medium for energy transfer, the electron temperature and the room temperature are not equal. Therefore, the coefficient k_d of the electron collision reaction under different gas pressures is no longer constant. Hence, the relationship between rate coefficient k_d and collision ionization coefficient α is given by:

$$k_d = \frac{\alpha w_e}{N} \tag{4}$$

where N is the particle concentration and w_e is the electron drift velocity.

$$w_e = \mu E \tag{5}$$

where u is the electron mobility that is inversely proportional to pressure p. The relationship among electron drift velocity w_e, electric field E, and air pressure p is as follows [14]:

$$w_e = a\frac{E}{p} \tag{6}$$

The relationship between the collision ionization coefficient α and the gas pressure p is given by [14]:

$$\alpha = A_1 p e^{(-B_1 p/E)} \tag{7}$$

where A_1 and B_1 are the constants determined by the nature of gas itself. Particle concentration N is proportional to the pressure p under a certain volume and temperature. Substituting (7) and (6) into (4) results in the following equation:

$$k_d = \frac{A_2 e^{-B_1 p/E} E}{p} \tag{8}$$

where A_2 is a constant.

For the primary reaction e + $SF_6 \rightarrow SF_{6\text{-}x}$ + xF + e ($x \leq 6$), the pure SF_6 concentration is larger than the concentration of primary products such as SF_2 and SF_4. Therefore, the primary reaction can be regarded as a "zero order reaction" [17] (i.e., the reaction rate is independent from the reactant concentration). The reaction rate is given by:

$$\frac{dc_d}{dt} = k_d \tag{9}$$

In the following equation, c_d is the concentration of the reaction product SF_x, and its relationship with time t is:

$$c_d = k_d t \tag{10}$$

SF_2 and SF_4 react with H_2O and O_2 molecules to produce SO_2F_2 and SOF_2 in the main gas zone of the regional decomposition model proposed by Van Brunt RJ [18]. According to chemical kinetics analysis, this reaction process is a chemical second-order reaction [19]. Its reaction rate is proportional to the product of the reactant concentrations [20], as follows:

$$\gamma = -\frac{d[SF_x]}{dt} = k_0[H_2O/O_2][SF_x] \tag{11}$$

where γ is the reaction rate; $[H_2O/O_2]$, $[SF_x]$ denote the reactant concentration; k_0 is the secondary reaction rate that is a pressure-independent and temperature-dependent coefficient according to the Arrhenius formula. The temperature of ions and molecules is equal to room temperature in the PD process [21]. Hence, k_0 can be considered as a constant in this experiment. Regardless of the chemical reaction to reach saturation, when the amount of SF_x generation is higher than that of consumption (i.e., when $t > Y/k_d$), given that $[H_2O/O_2]$ remains substantially unchanged for X during this period and the consumed concentration of SF_x is Y at time t, H_2O/O_2 and SF_x concentrations are $[H_2O/O_2] = X$ and $[SF_x] = k_d t - Y$, respectively. The reaction rate is as follows:

$$\gamma = \frac{d(k_d t - Y)}{dt} = k_0 X(k_d t - Y) \tag{12}$$

Equation (12) can be further derived as follows:

$$Y = k_d t - e^{-k_0 X t} \tag{13}$$

When t is sufficiently large, $e^{-k_0 X t} \rightarrow 0$, Equation (14) can be further derived as follows:

$$Y = k_d t \tag{14}$$

The concentration C of SO_2F_2 or SOF_2 is proportional to the consumed concentration Y of reactant SF_x. The voltage and electrode were consistent in all five experiments and thus, electric field E did not change. Therefore, the concentration of SO_2F_2 and SOF_2 can be expressed as follows:

$$C = \frac{Ae^{-Bp}}{p} t \tag{15}$$

where A and B are constants.

SOF_2, SO_2, and CO_2 of the free-metal particles defect were not discussed since they are almost free from the influence of gas pressure. The CO_2 formation process can also be explained by the collision theory, given that C atoms in metal protrusion defect are released by the collision between high energy particles. SO_2 is mainly derived from the hydrolysis of SOF_2 whose concentration versus the pressure's relationship curve is similar to that of SOF_2. Therefore, the relationship between the concentrations of CO_2, SO_2F_2, SOF_2, and SO_2 at 96 h in the metal protrusion defect, SO_2F_2 concentration in free-metal particles defect, and the pressure was approximately fitted by Equation (15). The fitting curves and expressions are presented in Figure 9 and Table 1, respectively.

Figure 9 shows that the fitting degree R^2 of the gas pressure of SOF_2, CO_2, and SO_2 concentrations at 96 h in metal protrusion defect, whose correlation curves of component concentration versus gas pressure present a Saturated Area, are lower than that of SO_2F_2, whose curve does not fall under the Saturated Area. This result is because the derivation process does not consider the saturation of the chemical reaction. However, the fitting degrees (R^2) of all decomposition components concentrations versus gas pressure are high, which indicates that the fitting curve fits well with the measured values. These results show that the derived formula can explain the relationship between the concentrations and the gas pressures of SO_2F_2, SOF_2, CO_2, and SO_2.

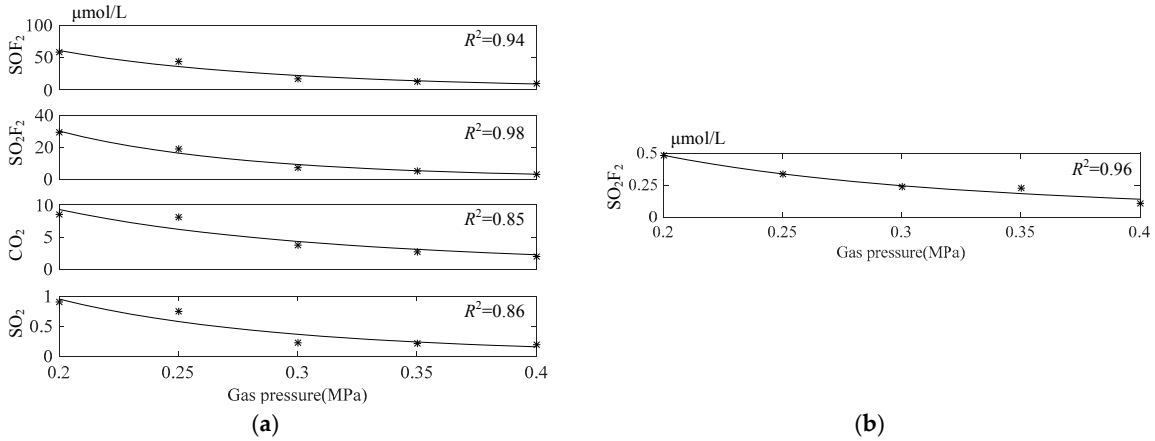

Figure 9. Correlation between 96 h concentration and gas pressure: (**a**) Protrusion and (**b**) particles.

Table 1. Fitting formula.

Typical Defects	96 h Component Fitting Formula
Metal Protrusion Defect	$C_{96h}(SOF_2) = \frac{40.34e^{-6.0p}}{p}$; $C_{96h}(SO_2F_2) = \frac{28.11e^{-7.7p}}{p}$; $C_{96h}(CO_2) = \frac{3.77e^{-3.54p}}{p}$; $C_{96h}(SO_2) = \frac{0.57e^{-5.47p}}{p}$;
Free metal Particles Defect	$C_{96h}(SO_2F_2) = \frac{0.17e^{-2.7p}}{p}$

5. Conclusions

To investigate the correlation between PD and gas pressure in the negative DC gas insulation equipment under two typical defects, SF_6 PD decomposition under different gas pressures were systematically implemented based on constructing the SF_6 decomposition experimental platform under DC PD. The following conclusions are drawn:

(1) SF_6 was decomposed into CO_2, SO_2F_2, SOF_2, and SO_2 in five groups of different gas pressures experiment under metal protrusion and free-metal particles defects. The yield relationship of metal protrusion defect is SOF_2 > SO_2F_2 > CO_2 > SO_2 under different gas pressures. The concentrations of SO_2F_2 and SOF_2 are much higher than others. The yield relationships of the free-metal particles defect under different pressures present a different relationship. The concentrations of SOF_2 are much higher than other concentrations.

(2) Under metal protrusion defect, the concentration of each decomposition component gradually decreases with increasing gas pressure. The change curves of SOF_2, CO_2, and SO_2 versus gas pressure can be divided into three stages, namely, Saturated, Exponent, and Flat Areas. Moreover, the change curves of SO_2F_2 can be broadly divided into two stages: Exponent and Flat Areas. The change curves of SOF_2, CO_2, and SO_2 versus gas pressure all fall under the Flat Area in metal free particles defect, whereas SO_2F_2 falls in the Exponent Area.

(3) Under the two typical defects, the effective characteristic ratio of c (SO_2F_2)/c (SOF_2 + SO_2) decreases as gas pressure increases. The pressure effect should be modified when GIS is used for fault diagnosis. The effective concentration ratio c (CO_2)/c (SO_2F_2 + SOF_2 + SO_2) gradually increases with the gas pressure and remains stable after 0.3 MPa. Therefore, the effect of gas pressure on the effective characteristic ratio of c (CF_4 + CO_2)/c (SO_2F_2 + SOF_2 + SO_2) can be neglected when GIS is used for fault diagnosis whose gas pressure falls within the range from 0.3 to 0.4 MPa.

(4) The relationship between the concentrations of CO_2, SO_2F_2, SOF_2, and SO_2 in the metal protrusion defect and the SO_2F_2 concentration in free-metal particles defect with the pressure can be expressed as $C = \frac{Ae^{-Bp}}{p}t$.

Acknowledgments: This study was supported by the Key Program of National Natural Science Foundation of China (51537009), National Natural Science Foundation of China (51607127), China Postdoctoral Science Foundation (Grant No. 2016T90723) and National Grid Corporation of China "Thousand Talents Program" special (National Grid Branch [2014] NO. 1192). We sincerely express our thankfulness here.

Author Contributions: Dong Yang, Ju Tang and Fuping Zeng conceived and designed the experiments; Dong Yang, Xu Yang, Ke Li, Lincong Chen, Qiang Yao, and Yulong Miao performed the experiments; Dong Yang, and Fuping Zeng analyzed the data; Dong Yang and Ju Tang wrote the paper.

Conflicts of Interest: The authors declare no conflict of interest.

References

1. Riechert, U.; Straumann, U.; Gremaud, R. Compact gas-insulated systems for high voltage direct current transmission: Basic design. In Proceedings of the IEEE/PES Transmission and Distribution Conference and Exposition (T&D), Dallas, TX, USA, 3–5 May 2016.
2. Ueta, G.; Okabe, S.; Utsumi, T.; Nukaga, J. Electric conductivity characteristics of FRP and epoxy insulators for GIS under DC voltage. *IEEE Trans. Dielectr. Electr. Insul.* **2015**, *22*, 2320–2328. [CrossRef]
3. Okabe, S.; Ueta, G.; Utsumi, T. Behavior of metallic particles in GIS under DC voltage. *IEEE Trans. Dielectr. Electr. Insul.* **2015**, *22*, 2889–2897. [CrossRef]
4. Ju, T.; Dong, Y.; Zeng, F.; Xiaoxin, Z. Research status of SF_6 insulation equipment fault diagnosis method and technology based on decomposed components analysis. *Trans. China Electrotech. Soc.* **2016**, *31*, 41–54.
5. Kokkoris, G.; Panagiotopoulos, A.; Goodyear, A.; Cooke, M.; Gogolides, E. A global model for SF_6 plasmas coupling reaction kinetics in the gas phase and on the surface of the reactor walls. *J. Phys. D Appl. Phys.* **2009**, *42*, 55209–55223. [CrossRef]

6. Girard, R.; Belhaouari, J.B.; Gonzalez, J.J.; Gleizes, A. A two-temperature kinetic model of SF_6 plasma. *J. Phys. D Appl. Phys.* **1999**, *32*, 2890–2901. [CrossRef]
7. Tang, J.; Liu, F.; Zhang, X.; Liang, X.; Fan, Q. Partial discharge recognition based on SF_6 decomposition products and support vector machine. *IET Sci. Meas. Technol.* **2012**, *6*, 198–204. [CrossRef]
8. Tang, J.; Zeng, F.; Pan, J.; Zhang, X. Correlation analysis between formation process of SF_6 decomposed components and partial discharge qualities. *IEEE Trans. Dielectr. Electr. Insul.* **2013**, *20*, 864–875. [CrossRef]
9. Kurte, R.; Beyer, C.; Heise, H.; Klockow, D. Application of infrared spectroscopy to monitoring gas insulated high-voltage equipment: Electrode material-dependent SF_6, decomposition. *Anal. Bioanal. Chem.* **2002**, *373*, 639–646. [CrossRef] [PubMed]
10. Tang, J.; Zeng, F.; Zhang, X.; Pan, J.; Yao, Q.; Hou, X.; Tang, Y. Relationship between decomposition gas ratios and partial discharge energy in GIS, and the influence of residual water and oxygen. *IEEE Trans. Dielectr. Electr. Insul.* **2014**, *21*, 1226–1234. [CrossRef]
11. Belarbi, A.; Pradayrol, C.; Casanovas, J.; Casanovas, A.M. Influence of discharge production conditions, gas pressure, current intensity and voltage type, on SF_6 dissociation under point-plane corona discharges. *J. Appl. Phys.* **1995**, *77*, 1398–1406. [CrossRef]
12. Tang, J.; Hu, Y.; Yao, Q.; He, J.; Zhang, X. Decomposition characteristics of SF_6 under partial discharge at different gas pressures. *High Volt. Eng.* **2014**, *40*, 2257–2263.
13. Purnomoadi, A.P.; Al-Suhaily, M.A.G.; Meijer, S.; Smit, J.J. The influence of free moving particles on the breakdown voltage of GIS under different electrical stresses. In Proceedings of the International Conference on Condition Monitoring and Diagnosis, Bali, Indonesia, 23–27 September 2012.
14. Raizer, Y.P. *Gas Discharge Physics*; Springer: Berlin, Germany, 1991; pp. 53–56.
15. Zeng, F.; Tang, J.; Zhang, X.; Sun, H. Study on the influence mechanism of trace H_2O on SF_6 thermal decomposition characteristic components. *IEEE Trans. Dielectr. Electr. Insul.* **2015**, *22*, 766–774. [CrossRef]
16. Chen, C.L.; Chantry, P.J. Photon-enhanced dissociative electron attachment in SF_6 and its isotopic selectivity. *J. Chem. Phys.* **1979**, *71*, 3897–3907. [CrossRef]
17. Tao, L.; Dong, H.; Zhong, H.; Jin, X.; Zhang, G. Influence factors of formation of decomposition by-products of SF_6 in 50 Hz AC corona discharge. *Trans. China Electrotech. Soc.* **2014**, *29*, 219–225.
18. Van Brunt, R.J.; Herron, J.T. Plasma chemical model for decomposition of SF_6 in a negative glow corona discharge. *Phys. Scr.* **2007**, *1994*, 9–29.
19. Tang, J.; Zeng, F.; Zhang, X.; Pan, J. Influence regularity of trace O_2 on SF_6 decomposition characteristics and its mathematical amendment under partial discharge. *IEEE Trans. Dielectr. Electr. Insul.* **2014**, *21*, 105–115. [CrossRef]
20. Liu, F.; Tang, J.; Liu, Y. Mathematical model of influence of oxygen and moisture on feature concentration ratios of SF_6 Decomposition Products. In Proceedings of the Power and Energy Society General Meeting, San Diego, CA, USA, 22–26 July 2012.
21. Peng, Q. Research of Plasma Chemical Model and Analysis of Influencing Factors of Streamer Discharge in Air. Ph.D. Thesis, Chongqing University, Chongqing, China, 2012.